IOPscience iopscience.iop.org

Home Search Collections Journals About Contact us My IOPscience

Magnetic excitations in the ordered phase of the antiferromagnetic alternating chain compound $CuWO_4$

This article has been downloaded from IOPscience. Please scroll down to see the full text article.

1996 J. Phys.: Condens. Matter 8 8613

(http://iopscience.iop.org/0953-8984/8/44/013)

View the table of contents for this issue, or go to the journal homepage for more

Download details:
IP Address: 171.66.16.207
The article was downloaded on 14/05/2010 at 04:26

Please note that terms and conditions apply.

J. Phys.: Condens. Matter **8** (1996) 8613–8634. Printed in the UK

Magnetic excitations in the ordered phase of the antiferromagnetic alternating chain compound $CuWO_4$

B Lake†, D A Tennant†, R A Cowley‡, J D Axe‡ and C K Chen†

† Oxford Physics, Clarendon Laboratory, Parks Road, Oxford OX1 3PU, UK
‡ Brookhaven National Laboratory, PO Box 5000, Upton, NY 11973-5000, USA

Received 13 May 1996, in final form 23 July 1996

Abstract. In this paper we present the results of a detailed experimental investigation of the magnetic excitations in the spin-$\frac{1}{2}$ Heisenberg antiferromagnet $CuWO_4$. Inelastic neutron scattering measurements made using a triple-axis spectrometer were performed in the low-temperature ordered phase and also briefly in the high-temperature phase at Brookhaven National Laboratory. The excitations in the ordered phase are compared to a spin-wave model and two possible sets of exchange paths are deduced, both of which provide good fits to the data. In both models $CuWO_4$ consists of weakly coupled alternating one-dimensional chains running in the $[2, -1, 0]$ direction. A calculation of the spin-wave intensities was also performed using the fitted exchange constants and agreement was found with the observed intensities. In the ordered phase, $CuWO_4$ has an energy gap at the zone centre and the excitations are well defined. Above the transition temperature constant-wavevector scans at the antiferromagnetic lattice points suggest the existence of a continuum of excitations.

1. Introduction

There has been a recent resurgence of interest in low-dimensional, spin-$\frac{1}{2}$ Heisenberg antiferromagnets. One reason for this is that high-T_c superconductors have been found to contain planes of $S = \frac{1}{2}$ copper ions and it is thought that understanding the magnetism in such systems may lead to an understanding of superconductivity. Another reason for the interest is that these antiferromagnets display interesting phenomena not found in three-dimensional magnets or ones with larger spin values. $KCuF_3$ is a good example of a spin-$\frac{1}{2}$ one-dimensional Heisenberg antiferromagnet. Spin-wave theory, which is the conventional theory for magnetic systems, predicts excitations which are well defined in energy; experiments on $KCuF_3$ however reveal that the excitations form a continuum [1]. In order to account fully for the strong quantum fluctations in $KCuF_3$ complex methods involving field theory have been introduced [2]. Another interesting low-dimensional antiferromagnet is $CuGeO_3$, which has alternating exchanges along the chain direction due to a spin–Peierls distortion. The excitations of $CuGeO_3$ display an energy gap at the zone centre in the spin–Peierls phase, and recent measurements indicate a continuum of excitations [3]. Neither of these features is predicted by spin-wave theory and at present there is no exact solution of the excitations in alternating chain systems.

$CuWO_4$ is a relatively little-studied crystal and its magnetic excitations have not been previously investigated by the technique of inelastic neutron scattering. Susceptibility measurements [4, 5], however, strongly suggest that it may exhibit low-dimensional magnetism. The susceptibility profile displays a broad maximum at temperatures around

0953-8984/96/448613+22$19.50 © 1996 IOP Publishing Ltd

90 K, far above the Néel temperature of 24 K; this indicates that $CuWO_4$ has magnetic short-range order well above its long-range ordering temperature as is characteristic of low-dimensional systems. Until now two groups of authors have made suggestions about the exchange interactions in $CuWO_4$. Doumerc *et al* [5] measured the susceptibility of a powdered sample and fitted it to the numerical calculations of Duffy and Barr [6], where the susceptibility of an infinite alternating chain is obtained by extrapolation from simulations of finite chains with lengths of up to ten spins. Forsyth *et al* [7] deduced the exchange interactions in $CuWO_4$ by examining the crystal structure; they concluded that there should be alternating chains in the $\boldsymbol{c}$ direction weakly coupled in the $\boldsymbol{b}$ direction.

In this paper we describe inelastic neutron scattering measurements of the excitations in the ordered phase of $CuWO_4$ and deduce the magnitude and direction of the exchanges. The rest of the paper is organized as follows: section 2 describes the experimental arrangement and section 3 the measurements performed. Section 4 is the analysis section where spin-wave theory is developed for a four-sublattice crystal (details are given in the appendix) and the results of fitting the excitations to this model are explained. Then in section 5 the results are discussed and the paper ends with a summary in section 6.

2. Experimental details

The structure of $CuWO_4$ is similar to that of the monoclinic family of Mn, Co, Fe and Ni tungstates but the action of a strong Jahn–Teller distortion is responsible for lowering its symmetry to triclinic, with space group $P\bar{1}$ [8]. The lattice parameters at 15 K are $a = 4.694(1)$, $b = 5.830(1)$ and $c = 4.877(1)$ Å and the unit cell angles are ($\alpha = 91.64(1)$, $\beta = 92.41(2)$ and $\gamma = 82.91(1)^\circ$ [7]. The Cu^{2+} ions in $CuWO_4$ have spin-$\frac{1}{2}$ and are responsible for the magnetic features of this compound. Figure 1 is a diagram of the chemical unit cell. It shows that there are two Cu^{2+} ions within each unit cell and they are related to each other by inversion symmetry. $CuWO_4$ exhibits long-range antiferromagnetic order below its transition temperature of 24.0 K [5]. The magnetic propagation vector has been measured by powder neutron diffraction [9] and single-crystal measurements [10] and is found to be (0.5, 0, 0) where the reciprocal lattice vectors are $\boldsymbol{a}^* = 2\pi(\boldsymbol{b}\times\boldsymbol{c})/(\boldsymbol{a}\cdot\boldsymbol{b}\times\boldsymbol{c})$, $\boldsymbol{b}^* = 2\pi(\boldsymbol{c}\times\boldsymbol{a})/(\boldsymbol{a}\cdot\boldsymbol{b}\times\boldsymbol{c})$ and $\boldsymbol{c}^* = 2\pi(\boldsymbol{a}\times\boldsymbol{b})/(\boldsymbol{a}\cdot\boldsymbol{b}\times\boldsymbol{c})$. The two Cu^{2+} ions within the unit cell align ferromagnetically at the spherical polar angles $\theta = 121^\circ$ and $\phi = 52^\circ$ where the polar axis is taken as being parallel to $\boldsymbol{c}$, and ϕ (is measured from $\boldsymbol{c}$–$\boldsymbol{a}^*$ plane [7]. This direction coincides with the axis of elongation of the Jahn–Teller distortion.

A batch of $CuWO_4$ crystals was grown in the Clarendon Laboratory, Oxford, using the flux growth technique where the flux of Li_2WO_4 was used. The relevant phase diagram is given in [11]. The starting materials CuO, WO_3 and Li_2CO_3 were heated to 1000 °C for 10 h. The mixture was then cooled at a rate of 2 °C h^{-1} to a temperature of 900 °C and at 0.5 °C h^{-1} to a temperature of 800 °C; after this cooling was continued at a faster rate. The crystal used for our measurements had a volume of $20 \times 20 \times 8$ mm^3 and consisted of two crystallites, one being half the size of the other. The two crystallites share a common face (0, 1, 0) and are related to each other by a 180° rotation about the $\boldsymbol{b}^*$ axis. The mosaic spread of the larger crystallite was 20′.

The inelastic neutron scattering measurements were made using the triple-axis spectrometers H7 and H8 at the High Flux Beam Reactor in Brookhaven National Laboratory, New York. The sample was mounted on the cold finger of a closed cycle refrigerator which could control the sample temperature to an accuracy of ±0.1 K above temperatures of 9 K. Pyrolitic graphite crystals were used for the monochromator and analyser to select neutron energies and wavelengths. For most of the experiment the

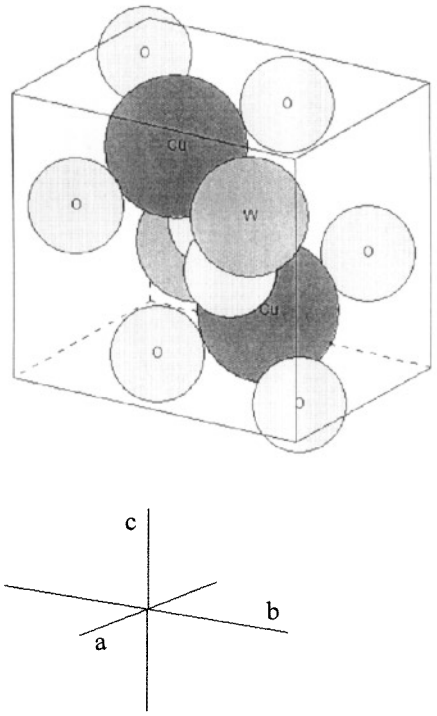

Figure 1. The chemical unit cell of $CuWO_4$.

final neutron energy was fixed at 14.7 meV and a pyrolitic graphite filter was placed after the sample to eliminate neutrons scattered by higher-order Bragg reflections in the monochromator. Collimators were used to determine the resolution and a typical collimation was 20′–20′–40′–40′ from reactor to detector. This arrangement provided us with a suitable energy range for measuring the excitations in the $\boldsymbol{a}^*$–$\boldsymbol{b}^*$ and $\boldsymbol{a}^*$–$\boldsymbol{c}^*$ planes of the crystal. For low-energy measurements a fixed incident neutron energy of 5 meV was used with a beryllium filter before the sample; this provided the high resolution required for a detailed investigation of the energy gap at the antiferromagnetic lattice points. All measurements were done in terms of monitor counts rather than time, so that the data were not affected by fluctations in the production of neutrons.

3. Measurements and results

Detailed measurements were made of the magnetic excitations in $CuWO_4$ at a temperature of 11 K, well below the ordering temperature of $T_N = 24.0$ K. Constant-wavevector and constant-energy scans were performed about the antiferromagnetic lattice points $(1.5, 0, 0)$, $(0.5, 1, -1)$ and $(0.5, 1, 0)$ in two scattering planes, the $\boldsymbol{a}^*$–$\boldsymbol{b}^*$ and $\boldsymbol{a}^*$–$\boldsymbol{c}^*$ planes, with a typical counting time of 6 min/data point. The neutron scattering data revealed spin-wave modes with well defined energies as shown in figure 2. The reasons that several peaks are often observed are firstly because there are two crystallites with different orientations and also because each crystallite produces two modes, a consequence of having four magnetic

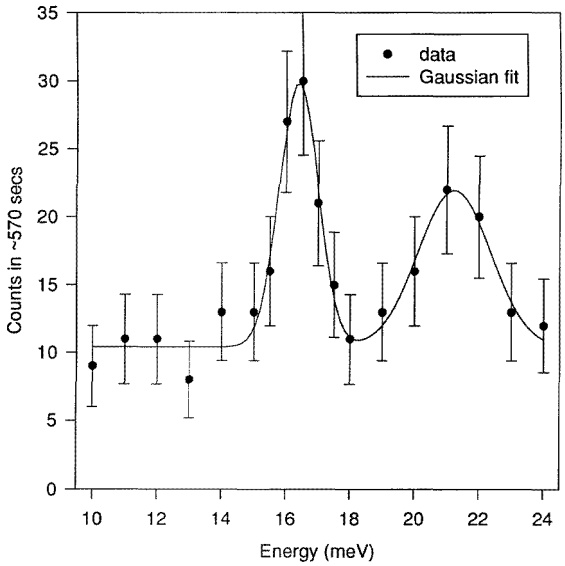

Figure 2. A constant-wavevector scan at $(1.5, -0.5, 0)$ using a counting time $\sim$ 570 s/data point. The peaks have been fitted to Gaussians and the extracted peak positions have been used as data points in the $\boldsymbol{b}^*$ dispersion, (figure 3(a)).

ions in the magnetic unit cell, as explained in section 4. Figure 2 shows a constant-wavevector scan at $(1.5, 0.5, 0)$. The peak at 16.59 meV has been identified as originating from the 'acoustic' mode of the larger crystallite and the peak at 21.12 meV from the 'optic' mode of the larger crystallite; the positions of these peaks have been used as data points in the $\boldsymbol{b}^*$ dispersion (figure 3(a)). Our measurements concentrated on the lower-energy acoustic mode of the larger crystallite, which we were able to identify because at the antiferromagnetic lattice points it produces the strongest scattering and has the lowest energy. This mode was followed outwards from the zone centre and mapped out in a large number of different high-symmetry directions. Gaussians were fitted to these scans to extract the peak positions and the dispersion relations for the excitations were built up as functions of wavevector. Some of the dispersions are shown in figures 3(a)–(e) where the dispersion direction quoted is that of the larger crystallite.

The errors shown in figures 3(a)–(e) are simply the errors in the peak positions from fitting the Gaussians. The best way to perform the peak fitting is in fact to fit the convolution of the four-dimensional resolution function with the spin-wave dispersion to the data; we did not do this because it requires a prior knowledge of the mode energies and dispersion relations in that region of reciprocal space. Simulations show that the resolution convolution can make the line-shape non-Gaussian and even asymmetric as is the case in some of our scans, thus fitting the profiles to Gaussians rather than the true line-shape can introduce small systematic errors. Simulations also show that in some cases the resolution can have the effect of shifting, by a small amount, the observed peak energy from the energy of the mode producing it; again this is not taken into account when fitting Gaussians. Another problem can arise when two modes come close to each other: their combined effect may produce just one peak in the data whose position corresponds to an energy in between that of the modes. The method we have used of fitting all the peaks to Gaussians to find the energies and errors treats all the scans consistently but underestimates the errors. A

reasonable estimation of the true errors is given by the scatter of the data points about the mean dispersion position.

The acoustic mode has an energy gap of 1.4 meV ($T = 13$ K) at the zone centre and its energy increases to 17 meV at the zone boundary in the $\boldsymbol{a}^*$ and $\boldsymbol{b}^*$ directions but to a lower energy of 8 meV in the $\boldsymbol{c}^*$ direction. The optic mode lies above the acoustic mode within an energy range of 10–22 meV. The data indicate that $CuWO_4$ has a direction of strong exchange in the $[2, -1, 0]$ direction figure 3(c), where the mode energies are large, while dispersions perpendicular to this direction are relatively low in energy (figures 3(d) and (e)), suggesting that the exchanges in these directions are weaker. At the antiferromagnetic lattice points investigated the intensity of the acoustic mode is at its greatest while the optic mode is too weak to be observed. When the modes are followed outwards in wavevector from the zone centre, large intensity changes are found in them with the optic mode often strongest at the zone boundary.

The temperature dependence of the order parameter for the antiferromagnetic phase transition in $CuWO_4$ was measured to determine the transition temperature. Figure 4 shows a graph of the integrated counts from the magnetic Bragg peak at $(2.5, 0, 0)$ as the temperature was varied from 13 to 26 K. This peak was chosen because it is weak with a maximum of 1515 counts s^{-1} at 13 K. The power law $y = A(T_N - T)^{2\beta}$ was fitted to the data in the region close to the transition temperature between 21 and 26 K; in this region all the count rates are less than 1000 counts per second and therefore the intensities are unlikely to be affected by extinction. The exponent $\beta = 0.214 \pm 0.022$ was extracted from the best fit, along with the Néel temperature $T_N = 24.00 \pm 0.03$ K. The value of the transition temperature is in agreement with that of Doumerc *et al* [5] but is higher than the 23.00 ± 0.02 K found by Forsyth *et al* [7]. The exponent β does not match the critical exponents of any simple theoretical model; it lies between the value of 0.34 for the order parameter of a three-dimensional magnet where the spins interact through Heisenberg exchange and the 0.125 expected for a two-dimensional Ising system, suggesting that the exchange interactions in $CuWO_4$ cause a complex cross-over from perfect three-dimensional behaviour.

The temperature dependence of the energy gap at the zone centre was investigated. In these measurements a fixed incident neutron energy of 5 meV was used for high resolution. Figure 5 shows two constant-wavevector scans at the antiferromagnetic lattice point $(0.5, 0, 0)$ for the temperatures 22 and 26K. At 22 K there is a well defined mode with an energy of 0.94 meV, well separated from the elastic Bragg peak which has a peak intensity of 5757 counts s^{-1}. By 26 K the Bragg peak has been replaced by a broad band of scattering which has a maximum of 1.82 counts s^{-1} at $E = 0.0$ meV and extends up in energy up to 1.5 meV; the energy gap is no longer apparent at this temperature. Below T_N the position of the energy gap was extracted from the scans. The full four-dimensional convolution of the resolution ellipsoid (calculated using the method of Cooper and Nathans [12]), with a spin-wave dispersion corresponding to that measured in this paper for $CuWO_4$ but where the size of the energy gap at the zone centre could be varied, was fitted to the data. In this calculation the usual $1/\omega$ spin-wave structure factor has been included, and the amount of thermal occupation of the energy mode at the temperatures of the scans is also taken into account. Details of the program used to calculate the resolution convolution can be found in [13]. The solid line in the 22 K graph (figure 5) is the fit to the data: it gives a somewhat narrower peak than is measured, indicating that at this temperature a degree of broadening is found in the energy mode. Figure 6 shows the energy gap as a function of temperature: its position decreases in energy as the temperature is increased; however it is unclear whether the gap tends to zero at the transition temperature or exists above T_N where it would be obscured by the quasi-elastic scattering.

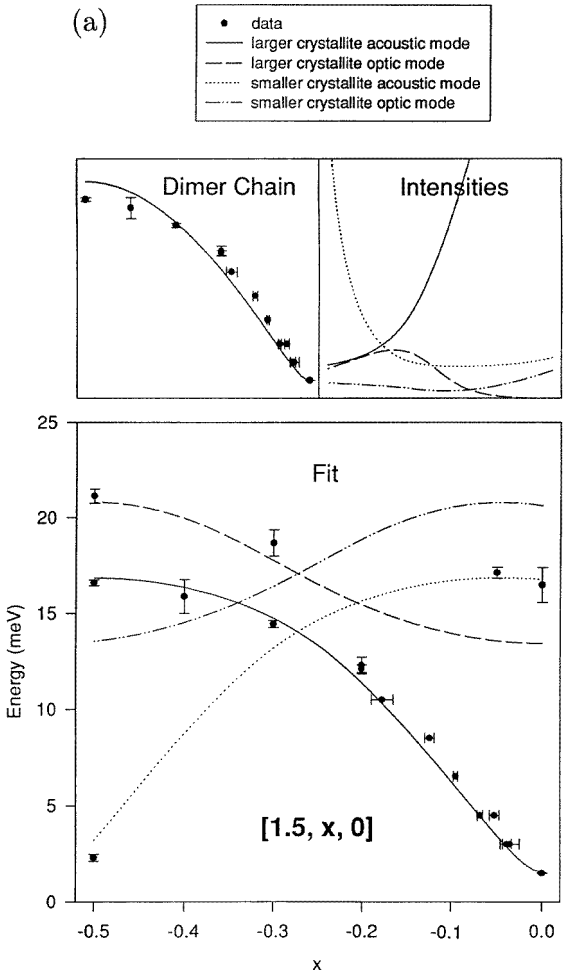

Figure 3. The spin-wave model fit to the data is shown in the bottom plots, where the dispersion direction given is that for the larger crystallite. The top right-hand graphs show the calculated intensities of the modes using the fitted parameters. The top left-hand plots show the fit of a model of uncoupled dimerized chains to the acoustic mode.

The solid line in figure 5 for the 26 K data is a simulation of the scattering expected from a spin-wave mode with no energy gap. The calculation is performed (as for the scans below T_N) by convolving the four-dimensional resolution ellipsoid with a spin-wave dispersion whose energy profile corresponds to that found in $CuWO_4$ in the ordered phase, but where the energy gap has been set to zero. As can been seen from the figure the peak in the calculated scattering intensity occurs at an energy of 0.4 meV. This and the asymmetric line-shape are due to the elongation of the vertical component of the resolution ellipsoid which enhances scattering at higher energies. The failure of the simulation suggests that the mode we measured at 26 K either has a structure factor which deviates from linear spin-wave theory or has a line-shape that is not well defined at this temperature.

We also briefly studied the excitations above T_N. The quasi-elastic scattering was measured in the two-axis configuration at 35 K in various directions in the $\boldsymbol{a}^*$–$\boldsymbol{b}^*$ plane. The

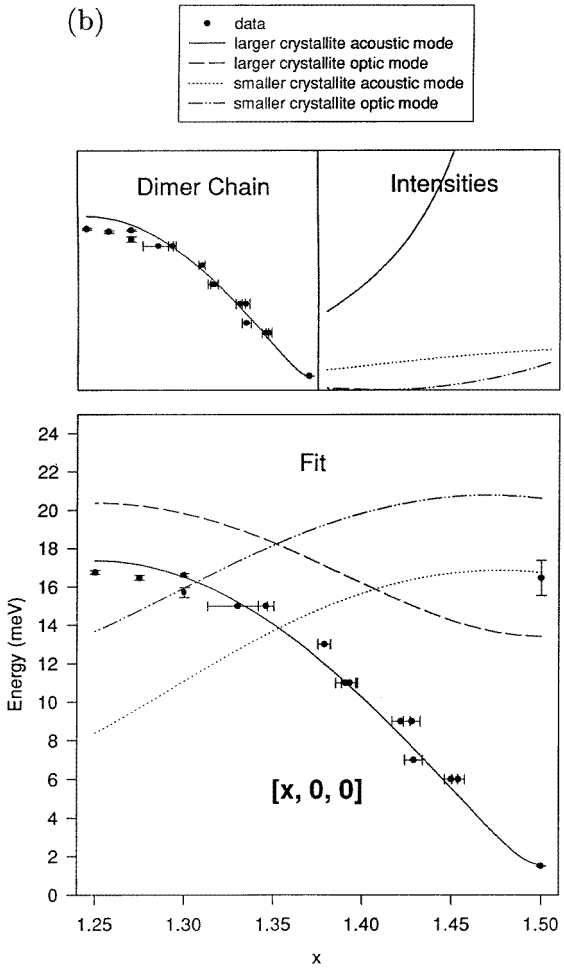

Figure 3. (Continued)

results show streaks of scattering in the [0.5, 1, 0] direction: this suggests the existence of short-range order above the transition temperature in the [2, −1, 0] direction. The excitations were also measured at 35 K in the $\boldsymbol{a}^*$ direction where a mode was found with energy similar to that of the acoustic mode below T_N but less well defined and of lower intensity.

4. Analysis

When $CuWO_4$ orders antiferromagnetically the unit cell is doubled in the $\boldsymbol{a}$ direction, leading to four Cu ions in each magnetic unit cell. Table 1 gives the positions of these ions (labelled 1–4) as fractions of the lattice parameters of the chemical unit cell [7] and the arrows indicate their relative ordering directions. Our aim was to discover which exchange interactions give rise to this ordering by studying the magnetic excitations.

There are many possible exchange paths in $CuWO_4$, because there are four Cu ions in the magnetic unit cell and all of the exchange interactions among them must be considered.

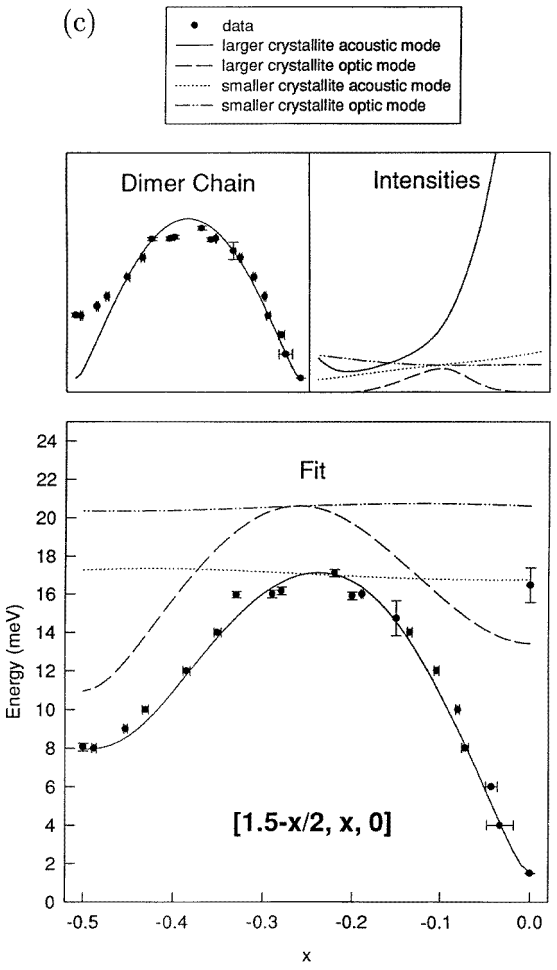

Figure 3. (Continued)

Table 1. The positions of the Cu ions within the magnetic unit cell are given as fractions of the lattice parameters of the chemical unit cell [7]. The arrows indicate the relative ordering of each Cu in the antiferromagnetic phase.

	Position of ion $R_{Cu} = l\boldsymbol{a} + m\boldsymbol{b} + n\boldsymbol{c}$			
Copper ion	l	m	n	Spin direction
Cu 1	0.495 37	0.659 42	0.245 24	↑
Cu 2	0.504 63	0.340 58	0.754 76	↑
Cu 3	1.495 37	0.659 42	0.245 24	↓
Cu 4	1.504 63	0.340 58	0.754 76	↓

Further, the low crystal symmetry means that there are a large number of independent exchange interactions. We have divided the possible interactions in $CuWO_4$ into four

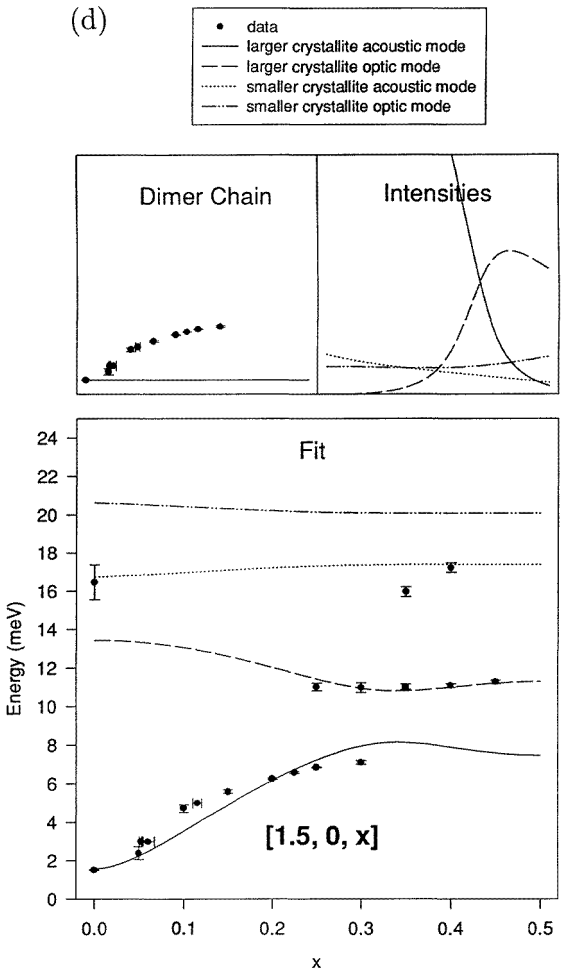

Figure 3. (Continued)

categories according to which ions are coupled, as listed in the first column of table 2. For example, the exchange represented by the category $J_{b[ijk]}$ links Cu 1 type ions to Cu 2 type ions and Cu 3 ions to Cu 4 ions. The vector $[i, j, k]$ gives the separation of the magnetic cells linked by the exchange where, since the indices are over the lattice parameters of the chemical cell, the index i changes in steps of two to correspond to the magnetic unit cell. Each exchange constant describes several exchange paths; for example if there is an exchange $J_{a[010]}$ linking the Cu 1 ions to the Cu 1 ions displaced one magnetic cell away in the $\boldsymbol{b}$ direction, then by symmetry the same exchange also describes the interaction between the Cu 2 ions and the Cu 2 ions displaced one magnetic unit cell away in the $\boldsymbol{b}$ direction, etc. The second column of table 2 lists the paths associated with each exchange constant. Finally, we have assumed that the exchange interactions linking Cu ions whose spins are aligned parallel to each other are ferromagnetic while those linking Cu ions whose spins are antiparallel are antiferromagnetic. Some example exchange paths in the $\boldsymbol{a}$–$\boldsymbol{b}$ plane are illustrated in figure 7.

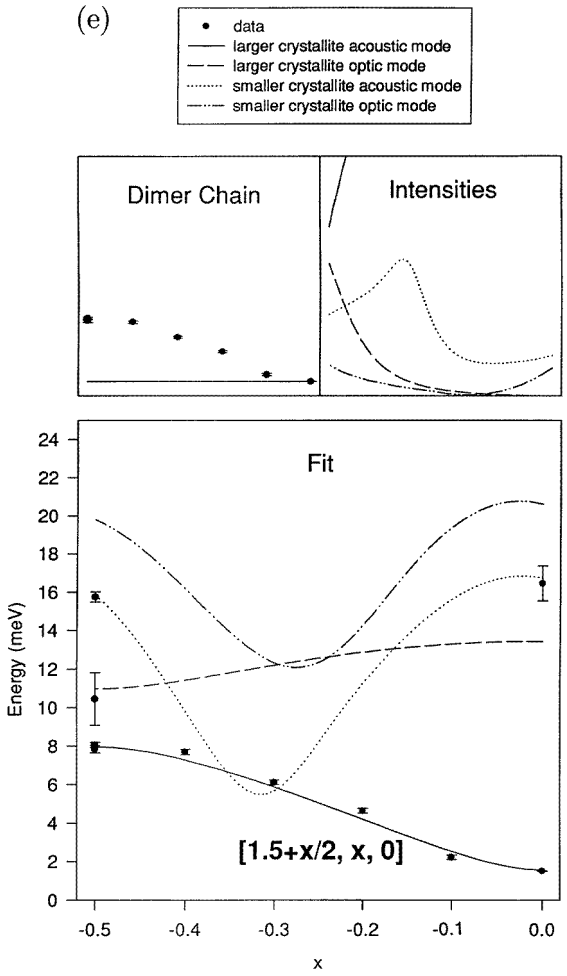

Figure 3. (Continued)

The general magnetic Hamiltonian for $CuWO_4$ can written as the sum of the Hamiltonians for each exchange category,

$$H = \sum_{r} \sum_{i,j,k} (H_{a\,r,[ijk]} + H_{b\,r,[ijk]} + H_{c\,r,[ijk]} + H_{d\,r,[ijk]}) \tag{1}$$

where $H_{a\,r,[ijk]}$ is the Hamiltonian involving the exchanges $J_{a[ijk]}$ and the sum over r is over all the magnetic unit cells in the crystal. The quantities $H_{a\,r,[ijk]}$ and $H_{b\,r,[ijk]}$ etc can be written explicitly in terms of the exchange interactions and spin operators as

$$\begin{aligned}
H_{a\,r,[ijk]} &= J_{a[ijk]}([S_{1,r} \cdot S_{1,(r+[i,j,k])}] + S_{2,r} \cdot S_{2,(r+[i,j,k])}] + [S_{3,r} \cdot S_{3,(r+[i,j,k])}] \\
&\quad + [S_{4,r} \cdot S_{4,(r+[i,j,k])}]) \\
H_{b\,r,[ijk]} &= J_{b[i,j,k]}([S_{1,r} \cdot S_{2,(r+[i,j,k])}] + [S_{3,r} \cdot S_{4,(r+[i,j,k])}]) \\
H_{c\,r,[ijk]} &= J_{c[i,j,k]}([S_{1,r} \cdot S_{3,(r+[i,j,k])}] + [S_{2,r} \cdot S_{4,(r+[i,j,k])}] \\
&\quad + [S_{3,r} \cdot S_{1,(r+[2+i,j,k])}] + [S_{4,r} \cdot S_{2,(r+[2+i,j,k])}]) \\
H_{d\,r,[ijk]} &= J_{d[i,j,k]}([S_{1,r} \cdot S_{4,(r+[i,j,k])}] + [S_{3,r} \cdot S_{2,(r+[2+i,j,k])}])
\end{aligned} \tag{2}$$

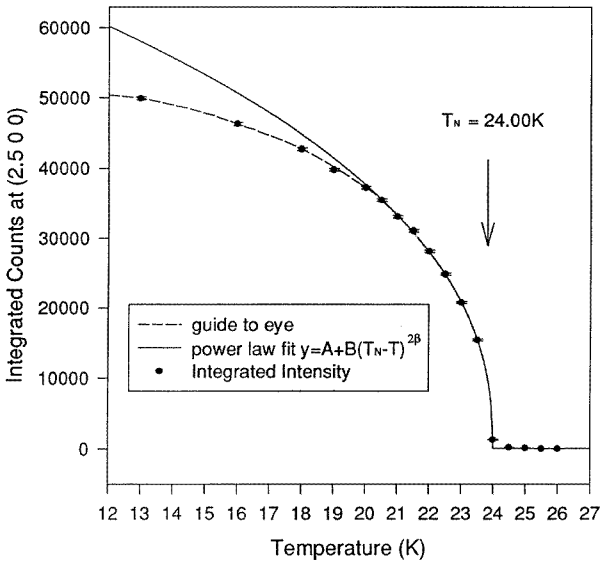

Figure 4. The integrated counts from the antiferromagnetic peak $(2.5, 0, 0)$, as the crystal is passed through the phase transition. The data points in the temperature range 21–26 K have been fitted to a power law expression indicated by the solid line; the dashed line is a guide to the eye.

Table 2. The exchange constants are given along with the ions that they couple and the interaction is described as ferromagnetic or antiferromagnetic; the vector $[i, j, k]$ refers to the magnetic unit cell.

Exchange	Ions linked	Type
$J_{a[ijk]}$	Cu 1 $\rightarrow$ Cu 1$[i, j, k]$	ferromagnetic
	Cu 2 $\rightarrow$ Cu 2$[i, j, k]$	
	Cu 3 $\rightarrow$ Cu 3$[i, j, k]$	
	Cu 4 $\rightarrow$ Cu 4$[i, j, k]$	
$J_{b[ijk]}$	Cu 1 $\rightarrow$ Cu 2$[i, j, k]$	ferromagnetic
	Cu 3 $\rightarrow$ Cu 4$[i, j, k]$	
$J_{c[ijk]}$	Cu 1 $\rightarrow$ Cu 3$[i, j, k]$	antiferromagnetic
	Cu 2 $\rightarrow$ Cu 4$[i, j, k]$	
	Cu 3 $\rightarrow$ Cu 1$[2+i, j, k]$	
	Cu 4 $\rightarrow$ Cu 2$[2+i, j, k]$	
$J_{d[ijk]}$	Cu 1 $\rightarrow$ Cu 4$[i, j, k]$	antiferromagnetic
	Cu 3 $\rightarrow$ Cu 2$[2+i, j, k]$	

where $S_{1,r}$ is the spin operator of the Cu 1 ion in the rth magnetic unit cell etc. For this Hamiltonian ferromagnetic exchange constants have negative values while antiferromagnetic exchange constants have positive values.

The excitations in $CuWO_4$ were modelled using spin-wave theory since this theory usually provides a good description of the excitations in three-dimensionally ordered magnets and predicts well defined energy modes like those observed in $CuWO_4$. The spin-wave calculation is described in the appendix; a general solution is found which can

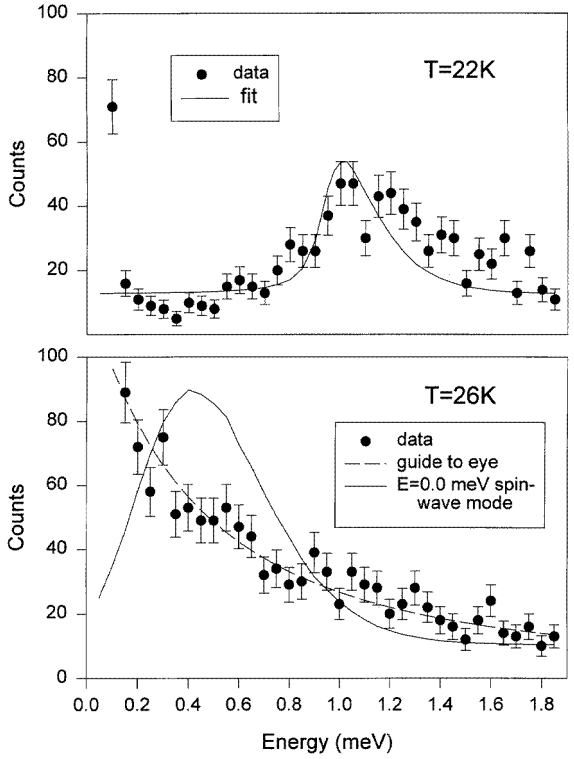

Figure 5. Constant-wavevector scans at (0.5, 0, 0) above and below T_N at 22 and 26 K. In the 22 K scan a mode is found at an energy $E = 0.94$ meV above the elastic Bragg peak. By 26 K only quasi-elastic scattering centred at $E = 0.0$ meV is found (maximum 182 counts s^{-1}).

deal with any number and combination of exchange interactions. Two sets of doubly degenerate modes are predicted by the theory: this is a direct consequence of having four magnetic ions in each magnetic unit cell in the same way that the number of phonon branches is related to the number of atoms in the unit cell. By analogy with the phonon case the lower mode is called the 'acoustic' mode and the upper mode the 'optic' mode.

The theoretical expressions for the spin-wave energies given by equations (A9), (A10) and (A5) were fitted to the measured dispersion relations by varying the values of the exchange constants. Only the acoustic mode of the larger crystallite was used in the fitting because this mode could be unambiguously followed up from the zone centre as described in section 3. For some of the other peaks observed it was unclear which crystallite they originated from. We also decided to restrict the exchange paths to those for which the separation between the copper ions was less than 7 Å as it is very unusual for exchange interactions to be significant for distances greater than this in an insulating crystal like $CuWO_4$. This condition left us with 14 remaining interactions. In order to further simplify the problem different planes in reciprocal space were fitted separately. For example the data in the $\boldsymbol{a}^*$–$\boldsymbol{b}^*$ plane were fitted separately from those in the $\boldsymbol{a}^*$–$\boldsymbol{c}^*$ plane, so that there were half the number of independent parameters in any one fit.

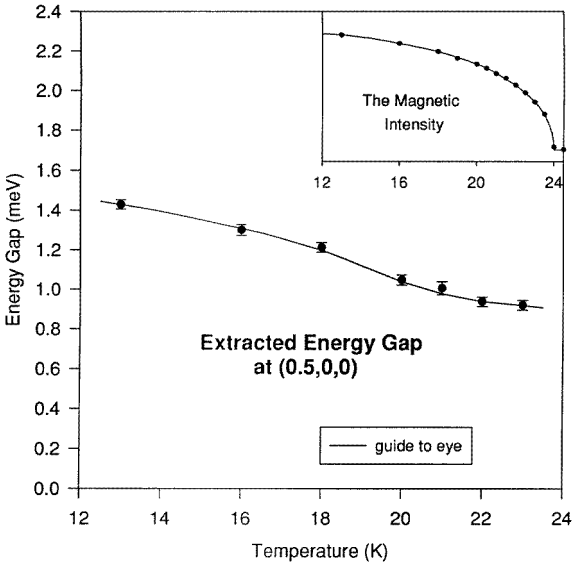

Figure 6. The energy gap at (0.5, 0, 0) as a function of temperature below T_N. The gap size was extracted from constant-wavevector scans at the zone centre. The top right-hand graph shows the behaviour of the integrated intensity from the antiferromagnetic Bragg peak at (2.5, 0, 0) over the same temperature region.

In addition to calculating the energies of the magnon modes their intensities were also calculated as functions of wavevector. The intensities are given by the neutron scattering cross-section

$$\frac{\mathrm{d}^2\sigma}{\mathrm{d}\Omega\,\mathrm{d}E'} \propto \frac{k'}{k}\int_{-\infty}^{+\infty}\sum_{\varepsilon,\gamma}(\delta_{\varepsilon\gamma}-\hat{Q}_\varepsilon\hat{Q}_\gamma)\sum_{p,\boldsymbol{r}}\sum_{p',\boldsymbol{r}'}\exp(-\mathrm{i}\boldsymbol{Q}\cdot(\boldsymbol{r}+\boldsymbol{d}p-\boldsymbol{r}'-\boldsymbol{d}p'))$$
$$\times\langle\langle S^{\varepsilon}_{p,\boldsymbol{r}}S^{\gamma}_{p',\boldsymbol{r}'}(t)\rangle\rangle\exp(-\mathrm{i}\omega t)\,\mathrm{d}t \qquad (3)$$

where the sum over p, $\boldsymbol{r}$ is over the pth ion in the $\boldsymbol{r}$th magnetic cell and the sum over ε, γ is over the co-ordinate x, y, z. The symbol $\boldsymbol{k}$ represents the initial wavevector $\boldsymbol{k}'$, the final wavevector and the wavevector transfer is given by $\boldsymbol{Q}=\boldsymbol{k}-\boldsymbol{k}'$, while the vector $\boldsymbol{d}(p)$ is the position of the pth Cu ion within the magnetic unit cell. The intensity calculation is performed by expressing the spin operators $S^{\varepsilon}_{p,\boldsymbol{r}}$ and $S^{\gamma}_{p',\boldsymbol{r}'}(t)$ in terms of the normal mode operators for $CuWO_4$. This calculation is outlined in the appendix.

Table 3. The exchange constants and their strengths for both models.

Model 1		Model 2	
Exchange	Strength (meV)	Exchange	Strength (meV)
$J_{d[-2,1,0]}$	33.26	$J_{d[0,0,-1]}$	31.27
$J_{d[0,0,0]}$	8.34	$J_{d[-2,1,-1]}$	9.01
$J_{b[0,1,0]}$	−0.52	$J_{b[0,1,0]}$	−3.09
$J_{b[0,0,-1]}$	−2.96	$J_{b[0,0,-1]}$	−0.55

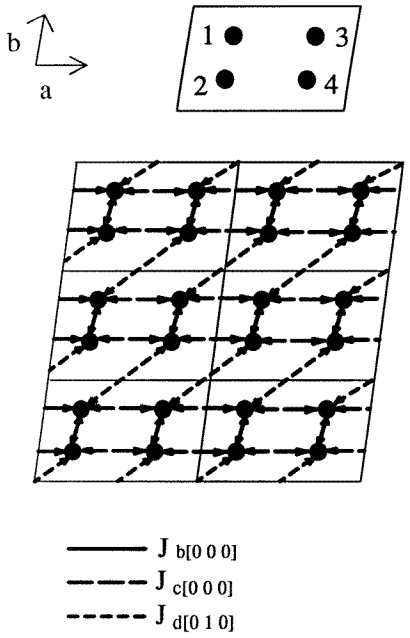

Figure 7. The exchange paths associated with three different exchange constants are drawn on the $\boldsymbol{a}$–$\boldsymbol{b}$ plane.

The process of fitting the exchange interactions and checking the intensities of the various models against the observed intensities led to two models which provide equally good fits to the data (see table 3). Both models consist of weakly coupled zig-zag dimerized chains running in the $[2, -1, 0]$ direction. The chains occupy alternating planes perpendicular to the $\boldsymbol{c}^*$ axis and are weakly coupled both within the planes and between the planes. Figure 8 shows the exchange paths of both models projected onto the $\boldsymbol{a}$–$\boldsymbol{b}$ and $\boldsymbol{a}$–$\boldsymbol{c}$ planes. Their projections are similar in the $\boldsymbol{a}$–$\boldsymbol{b}$ plane but in the $\boldsymbol{a}$–$\boldsymbol{c}$ plane the chains occupy different alternating layers. In model 1 the exchange interactions connect Cu ions within the magnetic cell whereas in model 2 the Cu ions in consecutive magnetic cells are connected. Figure 9(a) and 9(b) shows the dimerized chains for both models over several unit cells, with the double lines representing the strong intrachain exchange interaction, and the single lines the weak intrachain interaction. The reason why it is impossible to distinguish between these models from the excitations is because they are so similar. The only significant difference is that the chains in the two models occupy different alternating layers in the $\boldsymbol{c}$ direction; however the excitations are not affected by this.

In both models the larger intrachain exchange $J_{d[-2,1,0]}$ or $J_{d[0,0,-1]}$ is about 32 meV (where in the Hamiltonian, energy terms are given by $H = \sum_{1,1'} J_{1,1'} S_1 \cdot S_{1'}$ and $S = \frac{1}{2}$) and the weaker intrachain exchange $J_{d[0,0,0]}$ or $J_{d[-2,1,-1]}$ is about 8.5 meV. The interchain exchange interactions are about 2 meV in strength, however it is impossible to pinpoint which exchanges these are from the magnetic excitations because there are so many possible exchanges which would be equally satisfactory. Figure 3(a)–(e) shows the fits to the data; the calculation has been performed for both crystallites. In spite of the fact that only the acoustic mode of the larger crystallite was fitted, the calculated dispersions of the optic

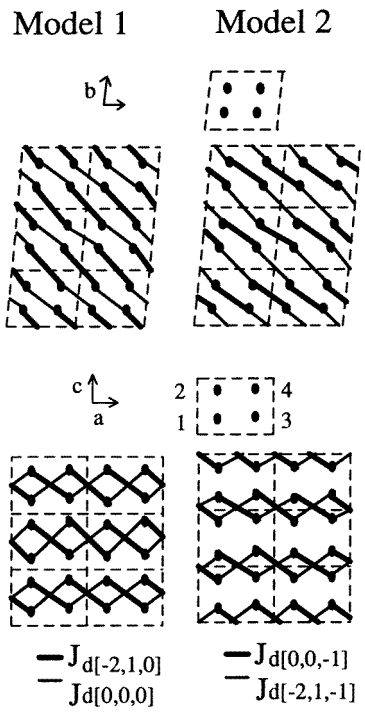

Figure 8. The projections onto the a–b plane and the a–c plane of the exchange interactions for the two models. On the a–b plane the models are very similar but on the a–c plane they occupy different alternating layers.

branch and the modes of the smaller crystallite (taking into account its different orientation) are found to correspond in frequency to the other peaks in the scattering data.

The intensities of the excitations were calculated using the fitted exchange constants; these are plotted with the fits in figure 3(a)–3(d) and provide an explanation as to why modes were observed at some points in reciprocal space and not others. For example in figure 3(d) the calculated intensity of the acoustic mode of the larger crystallite is predicted to be large around $x = 0.0$ and to decrease as x increases, while the optic mode of the larger crystallite is initially small but grows in intensity to be larger than the acoustic mode at the zone boundary. This explains why the acoustic mode was observed in the measurements from $x = 0.0$ to 0.3 but not for higher x, while the optic mode was observed for $x = 0.25$ to 0.5 but not for low values of x. In figure 3(a) the only mode not to be observed was the optic mode of the smaller crystallite: this can be explained by looking at the calculated intensities. Unfortunately in the region close to $x = 0.0$ where it may have been possible to observe this mode the measurements were not made at sufficiently high energies to detect it. In figure 3(e) the acoustic mode of the smaller crystallite was not found in the region $x = -0.2$ to $x = -0.4$ where it is predicted to be strong. This is because the intensity of the acoustic mode of the larger crystallite is much stronger as indicated on the intensity graph; however constant-wavevector scans at $x = -0.2$ and $x = -0.4$ are somewhat asymmetric in line-shape probably due to scattering from this mode.

Finally, in order to verify the idea that $CuWO_4$ consists of dimerized chains, a model of uncoupled alternating chains was compared to the data. This model produces just one

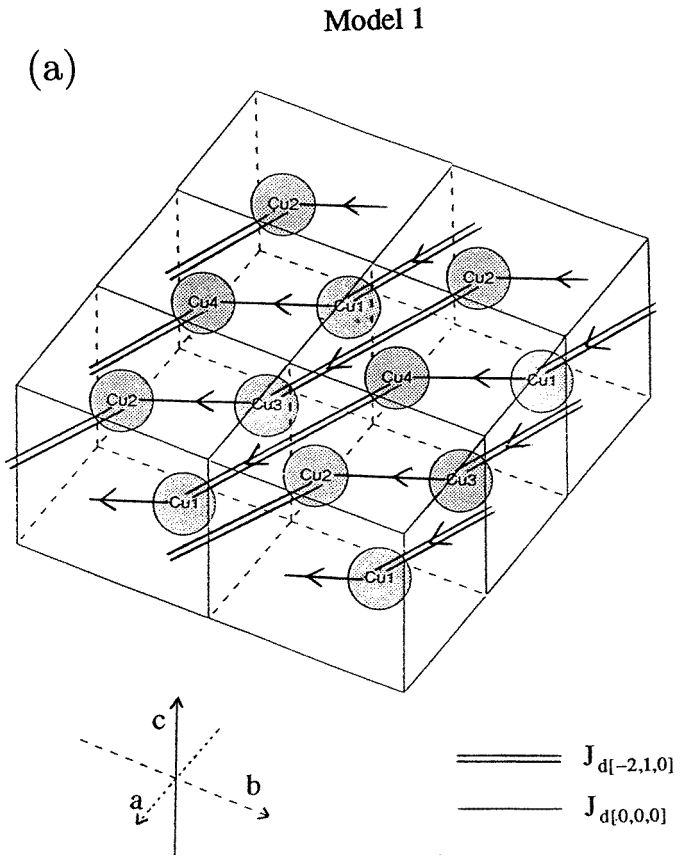

Figure 9. The intrachain exchange paths for the two models are shown over several chemical unit cells.

mode per crystallite because with the chains unconnected the neutrons no longer see the phase difference between them. This dispersion was fitted to the measured acoustic mode and the best fit resulted in a strong intrachain exchange interaction of 33.9 meV and a weak intrachain interaction of 9.6 meV; these values are similar to those obtained in the model with coupled chains. The fits, plotted in figure 3(*a*)–(*d*), closely follow the measured acoustic mode when the wavevector has a component in the chain direction, whereas when the wavevector is perpendicular to the chain direction the dispersion is zero for this model.

Some insight into why $CuWO_4$ consists of weakly coupled dimerized chains can be gained by considering the crystal structure. None of the possible exchange interactions in $CuWO_4$ could on their own magnetically couple together all the Cu ions either three dimensionally or two dimensionally, and only exchanges of the type $J_{c[i,j,k]}$ are capable of linking all the Cu ions in one dimension. In general a single exchange interaction would join Cu ions into pairs and these dimers would be magnetically isolated from each other: several different exchange interactions are needed for the Cu ions to be linked in either one, two or three dimensions. This feature of $CuWO_4$ is a direct consequence of the low crystal symmetry and the fact that it has four Cu ions in the magnetic unit cell. The three-dimensional ordering in $CuWO_4$ must therefore be produced by several different exchange interactions with different magnitudes and for this reason it is not suprising that the crystal is dimerized.

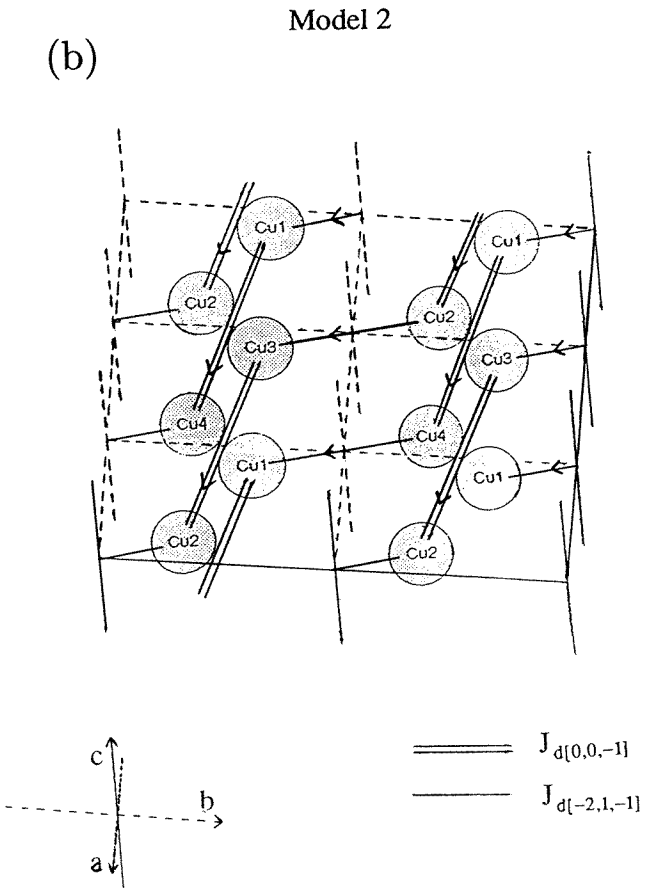

Figure 9. (Continued)

$CuWO_4$ is different from the other members of the tungstate family e.g. $MnWO_4$ and $CoWO_4$ for two reasons: firstly it is the only one to show low-dimensional magnetic behaviour and secondly it exhibits a strong Jahn–Teller distortion. The Jahn–Teller distortion in $CuWO_4$ causes the angle between the $\boldsymbol{a}$ and $\boldsymbol{b}$ axes to be changed from 90 to 82.91°: as a result, the diagonal distance $\boldsymbol{a}+\boldsymbol{b}$ is greater than the distance $\boldsymbol{a}-\boldsymbol{b}$. It is interesting to note that the antiferromagnetic chains run in the $[2,-1,0]$ direction, which is close to the direction of the shorter diagonal. The other tungstates, which do not have this distortion, also do not exhibit low-dimensional magnetism, which suggests that these two features of $CuWO_4$ are linked.

5. Discussion

The previous work on $CuWO_4$ is correct in predicting that magnetically it consists of chains with alternating exchange interactions; however, our results disagree with both the values of the exchange constants suggested by Doumerc *et al* [5] and the exchange paths of Forsyth *et al* [7]. Doumerc *et al* arrive at the idea of alternating chains by examining the crystal structure and measuring the susceptibility of a powdered sample. The $\boldsymbol{b}$–$\boldsymbol{c}$ plane

of $CuWO_4$ consists of zig-zag chains of CuO_6 octahedra separated from one another by chains of WO_6 octahedra. Doumerc *et al* suggested that one-dimensional magnetism would exist along these chains and that the exchange constants would alternate since successive coppers in the chains are non-equivalent as there are two coppers in each structural unit cell. We now know that these assumptions are incorrect: the one-dimensional chains lie not in the $\boldsymbol{b}$–$\boldsymbol{c}$ plane but in the $\boldsymbol{a}$–$\boldsymbol{b}$ plane. From their EPR measurements, Doumerc *et al* found the transition temperature to be 24 K and their inverse susceptibility data showed a broad minimum at 90 K corresponding to short-range order, which they assigned to the correlations within the alternating chains. They compared their data to the work of Duffy and Barr [6], whose exact numerical simulations of finite alternating chains of up to ten spins were extrapolated to predict the susceptibility of infinite chains. The values of the intrachain parameters given by Doumerc *et al* are 11.56 and 9.25 meV whereas we obtain 32 and 8.5 meV.

Forsyth *et al* [7] examined the structure of $CuWO_4$ and found a specific set of exchanges they believed would be responsible for the magnetic features. They assumed that antiferromagnetism was carried by the triple exchange path Cu–O–W–O–Cu first proposed by Mays [14] to account for the magnetic structure of $LiMnPO_4$. By measuring the angles at the intervening oxygens and the bond lengths they suggested three paths which combined together would produce alternating zig-zag chains in the $\boldsymbol{c}$ direction weakly coupled in the $\boldsymbol{a}$ direction. These exchange paths do not connect all the Cu ions and no coupling is predicted in the $\boldsymbol{b}$ direction. In contrast, our data show three-dimensional ordering, where the zone boundary excitation energy is large in both the $\boldsymbol{a}$ and $\boldsymbol{b}$ directions at 17 meV and is weaker in the $\boldsymbol{c}$ direction at 8 meV, immediately contradicting these exchange paths. We now know that the chain direction is $[2, -1, 0]$, not $[0, 0, 1]$ as Forsyth predicts. We conclude that for a complicated structure like that of $CuWO_4$ where the symmetry is triclinic the usual rules for predicting the triple exchange paths are not well obeyed and that it is neccessary to measure the spin-wave spectra to deduce the exchange constants.

As yet there is no complete theory of one-dimensional alternating spin-$\frac{1}{2}$ chains though there are numerous approximate theories [15–18] and experiments have been performed on the spin–Peierls system $CuGeO_3$. In its spin–Peierls phase $CuGeO_3$ consists of alternating chains in the $\boldsymbol{c}$ direction with exchange values 11.5 and 9.9 meV [18]. The chains are weakly coupled in the $\boldsymbol{b}$ direction by an exchange of 6% of that of the intrachain values and the exchange in the $\boldsymbol{a}$ direction is 0.3% of the intrachain exchanges: therefore the system is described as quasi-one-dimensional. A feature of $CuGeO_3$ is that it does not have a magnetically ordered phase [19]. One-dimensional spin-$\frac{1}{2}$ antiferromagnets are predicted never to order as there are not enough nearest neighbours per spin to stabilize the system. In practice, however, most crystals displaying one-dimensional behaviour do order at low enough temperatures because there is always some interchain coupling. The excitations of $CuGeO_3$ consist of a strong single mode forming the lower bound to a continuum [3]: this continuum is also a characteristic of one-dimensional spin-$\frac{1}{2}$ magnets. Finally $CuGeO_3$ has an energy gap at its zone centre [20, 21], a feature which has been predicted by theories of alternating chains and is a direct consequence of the dimerization.

$CuWO_4$ in contrast to $CuGeO_3$ does have a three-dimensionally ordered phase but the ordering temperature of 24 K is low compared to the intrachain exchange constants. This reflects the small magnitude of the interchain coupling responsible for the ordering. Our measurements have mostly concentrated on studying the ordered phase below T_N and not the disordered phase where $CuGeO_3$ has been investigated; however our constant-wavevector scans at the zone centre to measure the energy gap were performed both above and below T_N. The origin of the energy gap below T_N is unclear in that, while a gap is expected

above T_N due to quantum effects, this should go to zero in the ordered phase if there is no source of anisotropy. Possible causes of the energy gap are the dipole–dipole interactions between spins, or some intrinsic anisotropy, for example spin–orbit coupling if there is any residual unquenched orbital moment. The dipole–dipole interaction energy is proportional to the magnetization squared. If this interaction were the cause of the energy gap, the gap would drop to zero at T_N following the same function of temperature as the magnetic scattering intensity since the magnetic intensity is also proportional to the magnetization squared. Figures 4 and 6 demonstrate that this not the case; in addition calculations show that the dipole–dipole interaction energy is less than 0.05 meV, ruling out this interaction as the main cause of the energy gap.

Above T_N zone centre scans show a band of scattering that is wide in energy and is centred at $E = 0.0$ meV; as no energy gap is visible we can conclude that either there is no gap in the ordered phase or that the gap is small and is obscured by the quasi-elastic scattering. If the system turns out to have excitations like $CuGeO_3$ we would expect an energy gap and a continuum at the antiferromagnetic lattice points above T_N. The continuum would be occupied at these temperatures if the gap were less than 2 meV in size. If this is the case, a possible explanation for the broad energy band at $E = 0.0$ meV is that it results from scattering within a continuum. Figure 5 supports this argument: it shows a constant-wavevector zone centre scan at 26 K; the solid line is a simulation of the expected scattering from a well defined, spin-wave mode with no energy gap. This scattering is offset from $E = 0.0$ meV because of the effect of the vertical resolution as explained in section 3. The measured scattering clearly does not have this offset, showing that it cannot be produced by a well defined mode. Our brief exploration of the excitations above T_N revealed a dispersion similar to the acoustic mode below T_N but less well defined and of lower intensity again: one possibility is that some of the intensity has gone into a continuum.

Future work on $CuWO_4$ should first be to find out which of the two alternative sets of exchanges described in section 4 exists in the crystal and to try to understand the exchange mechanism. It would also be interesting to perform more measurements on $CuWO_4$ to find out exactly what happens to the energy gap and to explore the excitations above T_N.

6. Summary

In this paper the magnetic excitations of $CuWO_4$ have been studied in some detail by the technique of inelastic neutron scattering using a triple-axis spectrometer. Measurements were mostly carried out in the three-dimensionally ordered phase and revealed two well defined modes per crystallite; these were mapped out in a large number of high-symmetry directions. Fitting spin-wave theory to the dispersions leads to two different models which provide equally good fits to the data: both models consist of weakly coupled alternating chains in the $[2, -1, 0]$ direction where the intrachain exchange constants are 32 and 8.5 meV. The theoretical intensities of the dispersions using these exchange interactions explain why modes are observed at some wavevectors and not others. $CuWO_4$ is found to have an energy gap at the zone centre in its ordered phase and constant-wavevector scans suggest the existence of a continuum of excitations above T_N.

Acknowledgments

We have benefited from helpful discussions with J B Forsyth for which we are very grateful and we also wish to acknowledge B M Wanklyn for her assistance with the crystal growth.

We would like to thank Brookhaven National Laboratory, which provided us with beam time and made the experiments possible; our especial thanks go to R Rothe and J de la Rosa for the technical support they provided. The funding for this work came from EPSRC and the NATO travel fund. B Lake would like to thank Philips plc and in particular Dr P F Fewster for the CASE studentship.

Appendix

This appendix describes the calculation of the magnetic excitations in the ordered phase of $CuWO_4$ using spin-wave theory. The solution to the Hamiltonian given in equations (1) and (2) is found. This solution can accommodate any possible set of exchange interactions. Having found the spin-wave energies the method to compute the intensities of the excitations is outlined.

In the first stage of the spin-wave calculation the spin operators in the Hamiltonian undergo two transformations. The first transformation is to the spin deviation operators where a spin deviation exists on a spin if its value of S^z differs from that in its assumed Néel state. The transformation can be written as follows.

$$S^z_{p,\boldsymbol{r}} = \pm(S - a^+_{p,\boldsymbol{r}}a_{p,\boldsymbol{r}}) \qquad S^x_{p,\boldsymbol{r}} = \sqrt{(S/2)}(a_{p,\boldsymbol{r}} + a^+_{p,\boldsymbol{r}})$$
$$S^y_{p,\boldsymbol{r}} = \mp \mathrm{i}\sqrt{(S/2)}(a_{p,\boldsymbol{r}} - a^+_{p,\boldsymbol{r}}) \tag{A1}$$

where $p = 1$–4 is the index over the Cu sites and the upper sign is taken for sites 1 and 2 and the lower sign for sites 3 and 4. The operator $a^+_{p,\boldsymbol{r}}(a_{p,\boldsymbol{r}})$ creates (destroys) a spin deviation on the spin of the Cu ion of the pth type in the $\boldsymbol{r}$th magnetic unit cell.

The second transformation of the Hamiltonian is to the Fourier transform of the spin deviation operators and is given by

$$a^+_{p,\boldsymbol{r}} = \frac{1}{\sqrt{N}}\sum_{\boldsymbol{Q}} A^+_{p,\boldsymbol{Q}} \exp(\pm \mathrm{i}\boldsymbol{Q}(\boldsymbol{r} + \boldsymbol{d}(p)))$$
$$a_{p,\boldsymbol{r}} = \frac{1}{\sqrt{N}}\sum_{\boldsymbol{Q}} A_{p,\boldsymbol{Q}} \exp(\mp \mathrm{i}\boldsymbol{Q}(\boldsymbol{r} + \boldsymbol{d}(p))) \tag{A2}$$

where again $p = 1$–4 is the index over the Cu sites, the upper sign being taken for sites 1 and 2 and the lower sign for sites 3 and 4. The operator $A^+_{p,\boldsymbol{Q}}(A_{p,\boldsymbol{Q}})$ is the Fourier transform of the spin deviation creation (destruction) operator of sublattice p at wavevector $\boldsymbol{Q}$, and $\boldsymbol{d}(p)$ is the position of the pth Cu within the magnetic unit cell.

After these transformations the Hamiltonian can be written in the form

$$H = \sum_{\boldsymbol{Q}} H_{\boldsymbol{Q}}. \tag{A3}$$

If we just consider those terms that are quadratic in the operators $A_{\boldsymbol{Q}}$ and ignore higher-order terms the $H_{\boldsymbol{Q}}$ are

$$H_{\boldsymbol{Q}} = \tfrac{1}{2}\alpha_{\boldsymbol{Q},t,t'}A^+_{t,\boldsymbol{Q}}A^+_{t',\boldsymbol{Q}} + \tfrac{1}{2}\alpha^*_{\boldsymbol{Q},t,t'}A_{t,\boldsymbol{Q}}A_{t',\boldsymbol{Q}} + \beta_{\boldsymbol{Q},t,t'}A^+_{t,\boldsymbol{Q}}A_{t',\boldsymbol{Q}} \tag{A4}$$

where for $CuWO_4$ the $\alpha_{\boldsymbol{Q}t,t'}$ and $\beta_{\boldsymbol{Q},t,t'}$ are given by

$$\beta_{\boldsymbol{Q},1,1} = \beta_{\boldsymbol{Q},2,2} = \beta_{\boldsymbol{Q},3,3} = \beta_{\boldsymbol{Q},4,4} = S\sum_{i,j,k}(2J_{a[i,j,k]}(\cos(\boldsymbol{Q}\cdot[i,j,k]) - 1)$$
$$-J_{b[i,j,k]} + 2J_{c[i,j,k]} + J_{d[i,j,k]})$$

$$\beta_{\boldsymbol{Q},1,2} = \beta_{\boldsymbol{Q},2,1}{}^{*}\beta_{\boldsymbol{Q},3,4}{}^{*} = \beta_{\boldsymbol{Q},4,3} = S\sum_{i,j,k} J_{b[i,j,k]} \exp(-\mathrm{i}\boldsymbol{Q}\cdot(\boldsymbol{d}(2)+[i,j,k]-\boldsymbol{d}(1)))$$
$$\alpha_{\boldsymbol{Q},1,3} = \alpha_{\boldsymbol{Q},3,1} = \alpha_{\boldsymbol{Q},2,4} = \alpha_{\boldsymbol{Q},4,2} = 2S\sum_{i,j,k} J_{c[i,j,k]} \cos(\boldsymbol{Q}\cdot(\boldsymbol{d}(3)+[i,j,k]-\boldsymbol{d}(1)))$$
$$\alpha_{\boldsymbol{Q},2,3} = \alpha_{\boldsymbol{Q},3,2} = \alpha^{*}_{\boldsymbol{Q}1,4} = \alpha^{*}_{\boldsymbol{Q},4,1} = S\sum_{i,j,k} J_{d[i,j,k]} \exp(\boldsymbol{Q}\cdot(\boldsymbol{d}(2)+[i,j,k]-\boldsymbol{d}(3))). \quad \text{(A5)}$$

Vonsovskii [22] describes a general method of solving this Hamiltonian by introducing a third transformation to diagonalize it. This transformation is

$$A^{-}_{t,\boldsymbol{Q}} = \sum_{s}(\zeta^{-}_{s,\boldsymbol{Q}}u_{t,s,\boldsymbol{Q}} + \zeta^{+}_{s,\boldsymbol{Q}}v^{*}_{t,s,\boldsymbol{Q}}) \qquad A^{+}_{t,\boldsymbol{Q}} = \sum_{s}(\zeta^{+}_{s,\boldsymbol{Q}}u^{*}_{t,s,\boldsymbol{Q}} + \zeta^{-}_{s,\boldsymbol{Q}}v_{t,s,\boldsymbol{Q}}) \quad \text{(A6)}$$

where $\zeta^{+}_{s,\boldsymbol{Q}}(\zeta^{-}_{s,\boldsymbol{Q}})$ is the creation (annihilation) operator of the sth magnon mode. The $u_{t,s,\boldsymbol{Q}}$ and $v_{t,s,\boldsymbol{Q}}$ in equation (A6) are related to each other and the energies by the following set of homogeneous equations:

$$\sum_{t'}((\beta_{\boldsymbol{Q},t,t'} - E_{\boldsymbol{Q},s}\delta_{t,t'})u_{t',s,\boldsymbol{Q}} + \alpha_{\boldsymbol{Q},t,t'}v_{t',s,\boldsymbol{Q}}) = 0$$
$$\sum_{t'}(\alpha^{*}_{\boldsymbol{Q},t,t'}u_{t',s,\boldsymbol{Q}} + (\beta^{*}_{\boldsymbol{Q},t,t'} + E_{\boldsymbol{Q},s}\delta_{t,t'})v_{t',s,\boldsymbol{Q}}) = 0 \quad \text{(A7)}$$

where $E_{\boldsymbol{Q},s}$ is the energy of the sth magnon mode and the $u_{t',s,\boldsymbol{Q}}$ and $v_{t',s,\boldsymbol{Q}}$ are subject to the following conditions:

$$\sum_{t}(u_{t,s,\boldsymbol{Q}}u^{*}_{t,s',\boldsymbol{Q}} - v_{t,s,\boldsymbol{Q}}v^{*}_{t,s',\boldsymbol{Q}}) = \delta_{s,s'}$$
$$\sum_{t}(u_{t,s,\boldsymbol{Q}}v_{t,s',\boldsymbol{Q}} - u_{t,s',\boldsymbol{Q}}v_{t,s,\boldsymbol{Q}}) = 0. \quad \text{(A8)}$$

The equations (A7) form a matrix which can be diagonalized to find the magnon eigenvalues $E_{\boldsymbol{Q},s}$ and the eigenvectors $\{u_{t,s,\boldsymbol{Q}}, v_{t,s,\boldsymbol{Q}}\}$. For $CuWO_4$ we find that there are two sets of doubly degenerate modes with energies given by

$$E_{\boldsymbol{Q},1} = \sqrt{(C^{1}_{\boldsymbol{Q}} - C^{2}_{\boldsymbol{Q}})} \qquad E_{\boldsymbol{Q},2} = \sqrt{(C^{1}_{\boldsymbol{Q}} + C^{2}_{\boldsymbol{Q}})} \quad \text{(A9)}$$

where the quantities $C^{1}_{\boldsymbol{Q}}$ and $C^{2}_{\boldsymbol{Q}}$ are

$$C^{1}_{\boldsymbol{Q}} = \beta^{2}_{\boldsymbol{Q},1,1} - \alpha_{\boldsymbol{Q},4,1}\alpha^{*}_{\boldsymbol{Q},4,1} + \beta_{\boldsymbol{Q},1,2}\beta^{*}_{\boldsymbol{Q},1,2} - \alpha^{2}_{\boldsymbol{Q},1,3}$$
$$C^{2}_{\boldsymbol{Q}} = (4\beta^{2}_{\boldsymbol{Q},1,1}\beta_{\boldsymbol{Q},1,2}\beta^{*}_{\boldsymbol{Q},1,2} - 2\beta_{\boldsymbol{Q},1,2}\beta^{*}_{\boldsymbol{Q},1,2}\alpha_{\boldsymbol{Q},4,1}\alpha^{*}_{\boldsymbol{Q},4,1} + 4\alpha^{2}_{\boldsymbol{Q},1,3}\alpha_{\boldsymbol{Q},4,1}\alpha^{*}_{\boldsymbol{Q},4,1}$$
$$+(\alpha^{*}_{\boldsymbol{Q},4,1}\beta_{\boldsymbol{Q},1,2})^{2} + (\alpha_{\boldsymbol{Q},4,1}\beta^{*}_{\boldsymbol{Q},1,2})^{2} - 4\beta_{\boldsymbol{Q},1,1}\alpha^{*}_{\boldsymbol{Q},4,1}\alpha_{\boldsymbol{Q},1,3}\beta_{\boldsymbol{Q},1,2}$$
$$-4\beta_{\boldsymbol{Q},1,1}\alpha_{\boldsymbol{Q},4,1}\alpha_{\boldsymbol{Q},1,3}\beta_{\boldsymbol{Q},1,2}{}^{2})^{1/2}. \quad \text{(A10)}$$

The intensity of these excitations can also be calculated. The intensity is given by the neutron scattering cross-section equation (3). To perform the calculation the spin operators in equation (3) are written in terms of the magnon creation and annihilation operators for $CuWO_4$. To do this the $S^{\varepsilon}_{p,\boldsymbol{r}}$ and $S^{\gamma}_{p',\boldsymbol{r}'}(t)$ must undergo the same transformations that were used in the energy calculation: these transformations are given by equations (A1), (A2) and (A6). The neutron scattering cross-section can then be expressed in terms of the eigenvectors $u_{t,s,\boldsymbol{Q}}$ and $v_{t,s,\boldsymbol{Q}}$ which were obtained above. This method follows that of Lovesey [23] but is extended for the case of four magnetic ions in the magnetic unit cell.

References

[1] Tennant D A, Cowley R A, Nagler S E and Tsvelik A M 1995 *Phys. Rev.* B **52** 13 368–80
[2] Schultz H J 1986 *Phys. Rev.* B **34** 6372
[3] Lorenzo J E, Regnault L P, Hennion B, Aln M, Bourdarot F, Kulda J, Dhalenne G and Revcolevschi A at press
[4] Anders A G, Zvyagin A I, Kobets M I, Pelikh L N, Khats'ko E N and Yurko V G 1972 *Sov. Phys.–JETP* **35** 934
[5] Doumerc J P, Dance J M, Chaminade J P, Pouchard M, Hagemuller P and Krussanova M 1981 *Res. Bull.* **16** 985–90
[6] Duffy W and Barr K P 1968 *Phys. Rev.* **163** 165
[7] Forsyth J B, Wilkinson C and Zvyagin A I 1991 *J. Phys.: Condens. Matter* **3** 8433–40
[8] Kihlborg L and Gebert E 1970 *Acta Crystallogr.* B **2** 1020
[9] Weitzel H 1970 *Solid State Commun.* **8** 2071
[10] Wilkinson C and Sprague M J 1977 *Z. Kristallogr.* **145** 96
[11] Efremov V A and Trunov V K 1974 *Zh. Neorg. Khim.* **19** 501 (Engl. Transl. 1974 *Russ. J. Inorg. Chem.* **19** 272)
[12] Cooper M J and Nathans R 1973 *Acta. Crystallogr.* A **29** 160–9
[13] Tennant D A and McMorrow D F 1995 *Rescal for Matlab* World-Wide-Web site http://pc134.physics.ox.ac.uk/rescal/rescal.htm
[14] Mays J M 1963 *Phys. Rev.* **131** 38
[15] Bulaevskii L N 1963 *Zh. Eksp. Teor. Fiz.* **44** 1008 (Engl. Transl. 1963 *Sov. Phys.–JETP* **17** 684)
[16] Bonner J C and Blote H W J *Phys. Rev.* B **25** 6959
[17] Harris A B 1973 *Phys. Rev.* B **7** 3166
[18] Cowley R A, Lake B and Tennant D A 1996 *J. Phys.: Condens. Matter* **8** L179–L185
[19] Hase M, Terasaki I and Uchinokura K 1993 *Phys. Rev. Lett.* **70** 3651
[20] Pouget J P, Regnault J P, Ain M, Hennion J P, Veillot P, Dhalenne G and Revcolevschi A 1994 *Phys. Rev. Lett.* **72** 403
[21] Hirota K, Cox D E, Lorenzo J E, Shirane G, Tranquada J M, Hase M, Uchinokura K, Kojima H, Shibuya Y and Tanaka I 1994 *Phys. Rev. Lett.* **73** 736
[22] Vonsovskii S V *Magnetism* vol 2 (New York: Halsted–Wiley) ch 22
[23] Lovesey S W 1987 *Theory of Neutron Scattering from Condensed Matter* (Oxford: Clarendon)